Synthesis and characterization of di-nuclear bis(benzotriazole iminophenolate) cobalt complexes: catalysis for copolymerization of carbon dioxide with epoxides

Yu-Chia Su,[a] Chen-Yen Tsai,[b] Li-Shin Huang[a], Chia-Her Lin[c] and Bao-Tsan Ko*[a]

[a]*Department of Chemistry, National Chung Hsing University, Taichung 402, Taiwan*

[b]*Department of Chemistry, Chinese Culture University, Taipei 111, Taiwan*

[c]*Department of Chemistry, Chung Yuan Christian University, Chung-Li 32023, Taiwan*

Fig. S1 UV–Vis spectra of complexes **1**–**6** in CH_2Cl_2 ($[M]_0$ = 20 μM) at 25 °C.

Fig. S2 Mass spectrum of di-cobalt complex **1** was obtained using positive electron spray ionization (ESI^+) technique.

Fig. S3 Mass spectrum of di-cobalt complex **6** was obtained using positive electron spray ionization (ESI^+) technique.

Fig. S4 ORTEP drawing of complex **2** with probability ellipsoids drawn at level 50%. Hydrogen atoms are omitted for clarity.

Fig. S5 ORTEP drawing of complex **3** with probability ellipsoids drawn at level 50%. Hydrogen atoms are omitted for clarity.

Fig. S6 ORTEP drawing of complex **4** with probability ellipsoids drawn at level 50%. Hydrogen atoms are omitted for clarity.

Fig. S7 ORTEP drawing of complex **5** with probability ellipsoids drawn at level 50%. Hydrogen atoms are omitted for clarity.

Fig. S8 Plot of M_n (■) and PDI (▲) (determined from GPC analysis) *versus* CHO conversion for the copolymerization of CO_2 and CHO using di-cobalt complex **1** as the catalyst ($[CHO]_0/[\mathbf{1}]_0$ = 1600) at 110 °C and 3.45 MPa CO_2.

Fig. S9 GPC traces for the produced PCHC with a bimodal molecular weight distribution catalyzed by di-cobalt **1** (Table 2, entry 6).

Fig. S10 GPC traces for the produced PCHC polyol with a unimodal molecular weight distribution catalyzed by di-cobalt **1** (Table 2, entry 15).

Fig. S11 ^{1}H NMR spectrum of the purified copolymer produced by utilizing di-cobalt complex **1** (Table 2, entry 16) in $CDCl_3$. Peak at δ 4.5−4.9 ppm is assigned to the methine protons in PVCHC, and no significant signal at 3.4−3.8 ppm suggests >99% carbonate repeated units in PVCHC.

Fig. S12 ^{1}H NMR spectrum of the crude product (Table 2, entry 18) from the reaction mixture of CPO/CO_2 copolymerization by using di-Co complex **1** in $CDCl_3$.

Fig. S13 ^{1}H NMR spectrum of the purified copolymer afforded by utilizing di-cobalt complex **1** (Table 2, entry 17) in $CDCl_3$. Peak at δ = 4.93 ppm is assigned to the methine protons in PCPC, and no obvious signal at 3.6–4.0 ppm confirms >99% carbonate linkages in PCPC.

Fig. S14 GPC traces for the produced PCHC polyol with a unimodal molecular weight distribution catalyzed by di-Co **1** in the presence of neopentyl glycol as the CTA (Table 3, entry 2).

Fig. S15 MALDI-TOF spectrum of the produced PCHC polyol catalyzed by di-Co complex **1** in the presence of neopentyl glycol as the CTA (Table 3, entry 2).

Fig. S16 MALDI-TOF spectrum of the produced PCHC polyol catalyzed by di-Co complex **1** in the presence of BDO as the CTA (Table 3, entry 1).

Fig. S17 MALDI-TOF spectrum of the produced PCHC polyol catalyzed by di-Co complex **1** in the presence of BDO as the CHD (Table 3, entry 3).

Fig. S18 ^{1}H NMR spectrum ($CDCl_3$) of the purified PCHC polyol catalyzed by di-cobalt complex **1** in the presence of BDO (Table 3, entry 1).

Fig. S19 ^{1}H NMR spectrum ($CDCl_3$) of the purified PCHC polyol catalyzed by di-cobalt complex **1** in the presence of CHD (Table 3, entry 3).

Fig. S20 GPC traces of PCHC polyol samples produced by di-Co complex **1** on increasing the

[neopentyl glycol]$_0$/[**1**]$_0$ ratio in a range of 40-150.

Table S1 Key absorbance characteristics for UV–Vis spectra of complexes **1–6** in CH_2Cl_2 ([M]$_0$ = 20 μM) at 25 °C

Table S2 Crystallographic data of complexes **1-6**

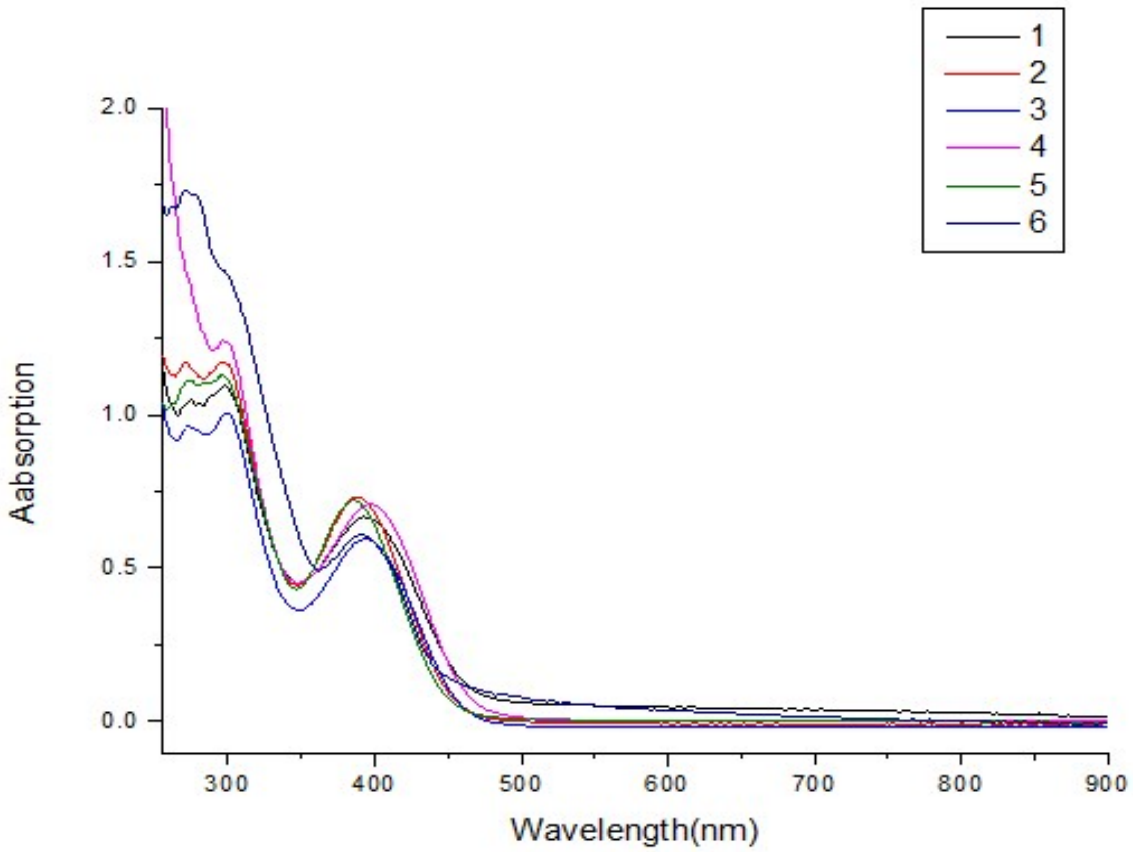

Fig. S1 UV–Vis spectra of complexes **1**–**6** in CH_2Cl_2 ($[M]_0$ = 20 μM) at 25 °C.

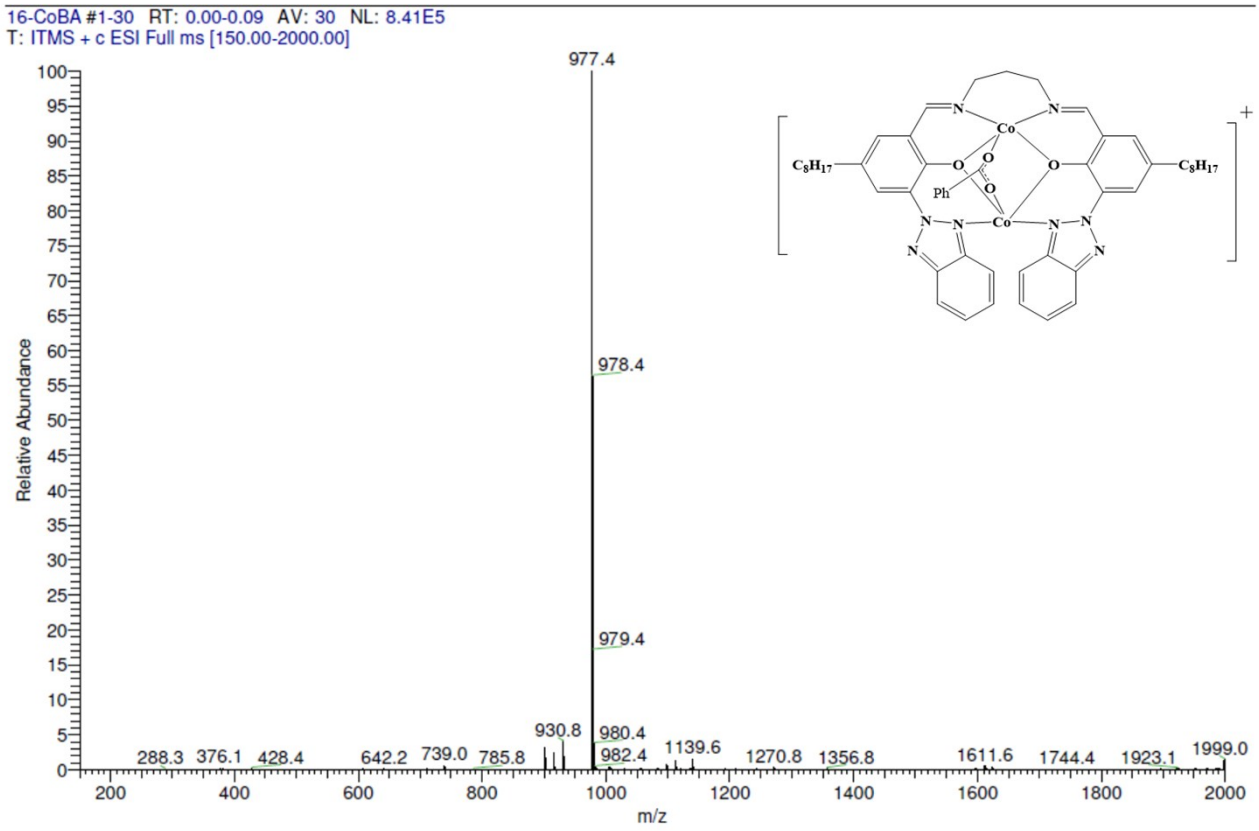

Fig. S2 Mass spectrum of di-cobalt complex **1** was obtained using positive electron spray ionization (ESI^+) technique.

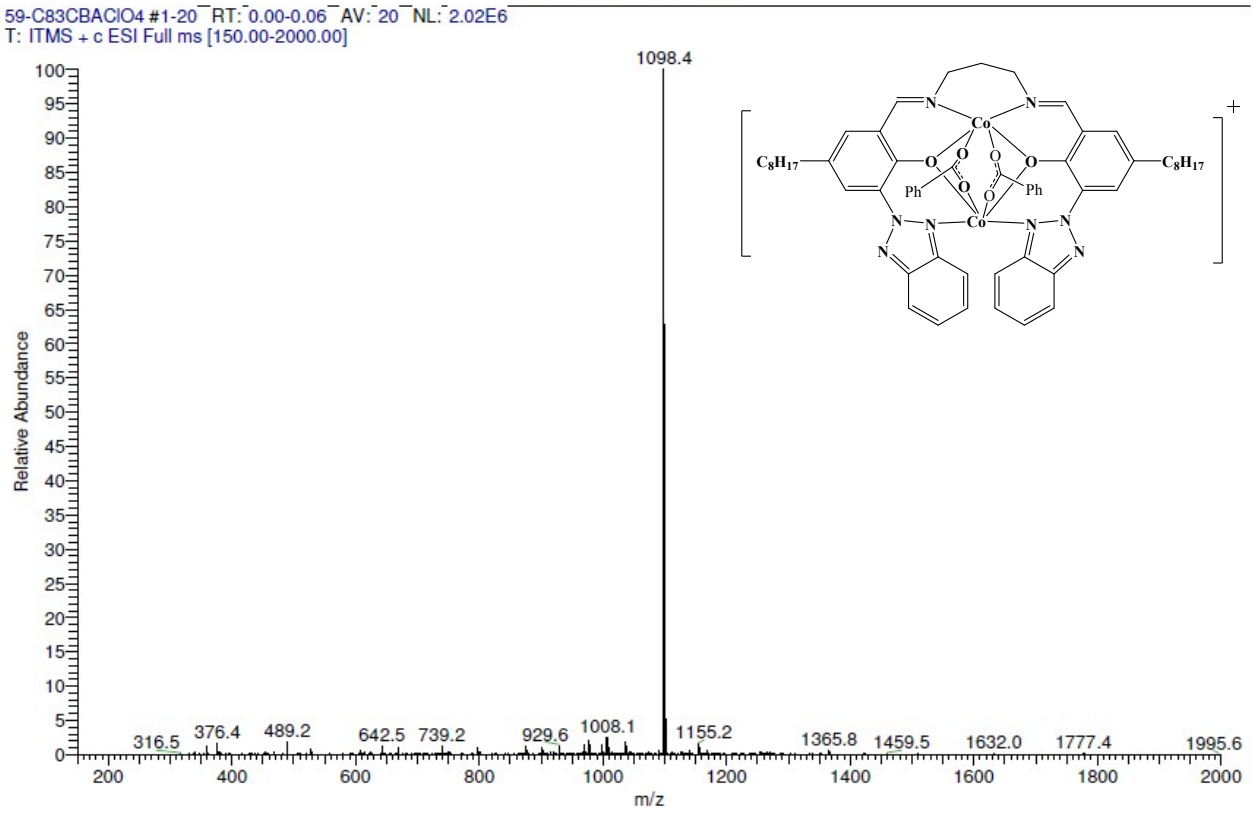

Fig. S3 Mass spectrum of di-cobalt complex **6** was obtained using positive electron spray ionization (ESI^+) technique.

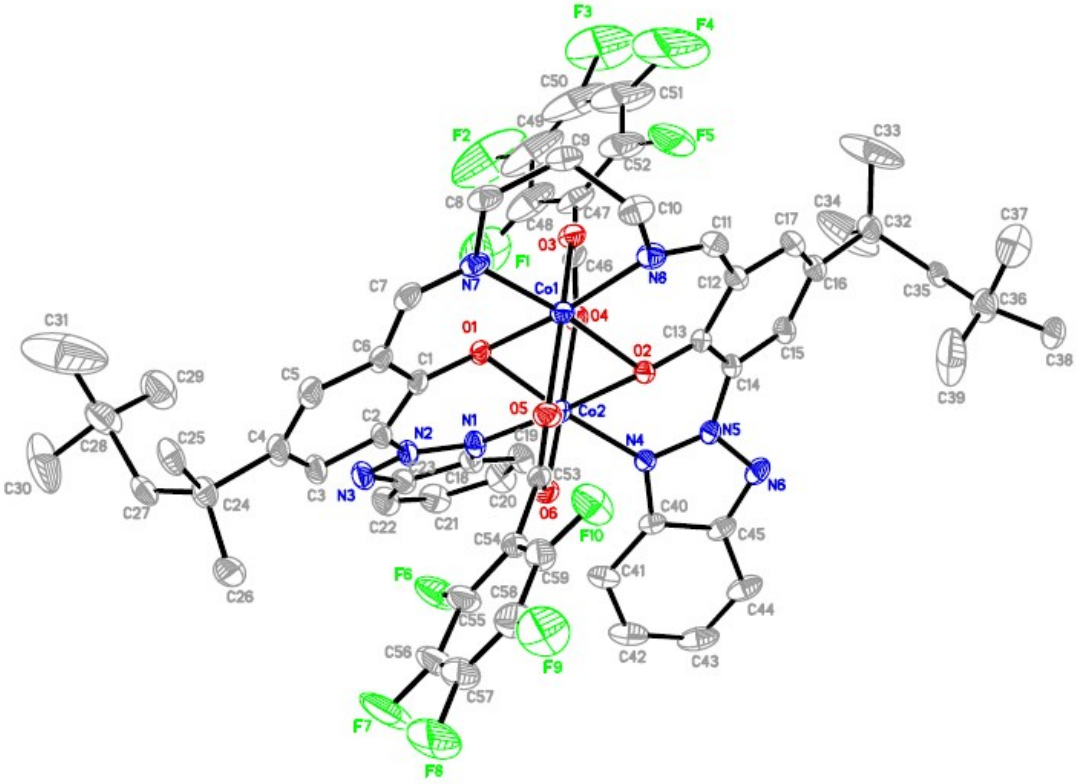

Fig. S4 ORTEP drawing of complex **2** with probability ellipsoids drawn at level 50%. Hydrogen atoms are omitted for clarity. Selected bond lengths (Å) and angles (deg): Co(1)-O(1) 2.0557(15), Co(1)-N(8) 2.0667(19), Co(1)-O(2) 2.0699(13), Co(1)-N(7) 2.0846(17), Co(1)-O(5) 2.1297(14), Co(1)-O(3) 2.1730(14), Co(2)-O(2) 2.0692(14), Co(2)-O(1) 2.0730(13), Co(2)-N(4) 2.0832(16), Co(2)-N(1) 2.0937(17), Co(2)-O(6) 2.0991(14), Co(2)-O(4) 2.1148(15), O(1)-Co(1)-N(8) 169.08(6), O(1)-Co(1)-O(2) 93.69(5), N(8)-Co(1)-O(2) 85.45(6), O(1)-Co(1)-N(7) 86.83(6), N(8)-Co(1)-N(7) 95.75(7), O(2)-Co(1)-N(7) 170.87(6), O(1)-Co(1)-O(5) 85.66(6), N(8)-Co(1)-O(5) 105.03(7), O(2)-Co(1)-O(5) 83.53(6), N(7)-Co(1)-O(5) 87.42(6), O(1)-Co(1)-O(3) 81.12(6), N(8)-Co(1)-O(3) 87.96(7), O(2)-Co(1)-O(3) 86.55(5), N(7)-Co(1)-O(3) 102.52(6), O(5)-Co(1)-O(3) 162.92(6), O(2)-Co(2)-O(1) 93.20(5), O(2)-Co(2)-N(4) 83.33(6), O(1)-Co(2)-N(4) 175.32(6), O(2)-Co(2)-N(1) 175.08(6), O(1)-Co(2)-N(1) 81.90(6), N(4)-Co(2)-N(1) 101.59(7), O(2)-Co(2)-O(6) 84.85(6), O(1)-Co(2)-O(6) 86.10(5), N(4)-Co(2)-O(6) 96.68(6), N(1)-Co(2)-O(6) 94.33(6), O(2)-Co(2)-O(4) 85.79(6), O(1)-Co(2)-O(4) 84.50(5), N(4)-Co(2)-O(4) 92.09(6), N(1)-Co(2)-O(4) 94.15(6), O(6)-Co(2)-O(4) 166.34(6).

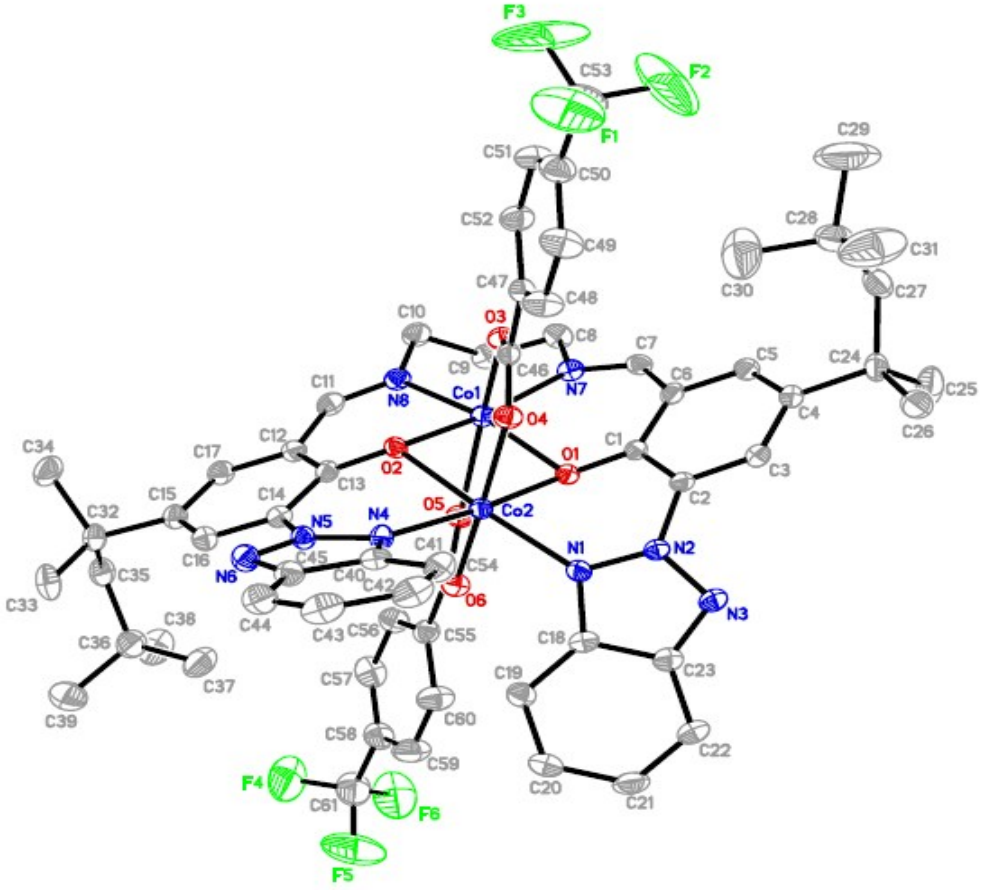

Fig. S5 ORTEP drawing of complex **3** with probability ellipsoids drawn at level 50%. Hydrogen atoms are omitted for clarity. Selected bond lengths (Å) and angles (deg): Co(1)-O(1) 2.0401(16), Co(1)-O(2) 2.0414(16), Co(1)-N(8) 2.075(2), Co(1)-N(7) 2.092(2), Co(1)-O(3) 2.1843(17), Co(1)-O(5) 2.2338(17), Co(2)-O(6) 2.0434(17), Co(2)-O(4) 2.0449(17), Co(2)-O(2) 2.0771(16), Co(2)-O(1) 2.0945(16), Co(2)-N(4) 2.095(2), Co(2)-N(1) 2.100(2), O(1)-Co(1)-O(2) 93.98(6), O(1)-Co(1)-N(8) 166.09(7), O(2)-Co(1)-N(8) 87.39(7), O(1)-Co(1)-N(7) 86.33(7), O(2)-Co(1)-N(7) 169.35(7), N(8)-Co(1)-N(7) 94.87(8), O(1)-Co(1)-O(3) 86.28(6), O(2)-Co(1)-O(3) 80.98(6), N(8)-Co(1)-O(3) 107.60(7), N(7)-Co(1)-O(3) 88.42(7), O(1)-Co(1)-O(5) 80.32(6), O(2)-Co(1)-O(5) 83.09(6), N(8)-Co(1)-O(5) 86.12(7), N(7)-Co(1)-O(5)107.42(7), O(3)-Co(1)-O(5) 158.37(6), O(6)-Co(2)-O(4) 170.00(7), O(6)-Co(2)-O(2) 86.88(6), O(4)-Co(2)-O(2) 6.29(6), O(6)-Co(2)-O(1) 86.82(7), O(4)-Co(2)-O(1) 86.06(6), O(2)-Co(2)-O(1) 91.36(6), O(6)-Co(2)-N(4) 92.82(7), O(4)-Co(2)-N(4) 93.51(7), O(2)-Co(2)-N(4) 82.51(7), O(1)-Co(2)-N(4) 173.87(7), O(6)-Co(2)-N(1) 90.28(7), O(4)-Co(2)-N(1) 95.59(7), O(2)-Co(2)-N(1) 172.41(7), O(1)-Co(2)-N(1) 81.46(7), N(4)-Co(2)-N(1) 104.67(8).

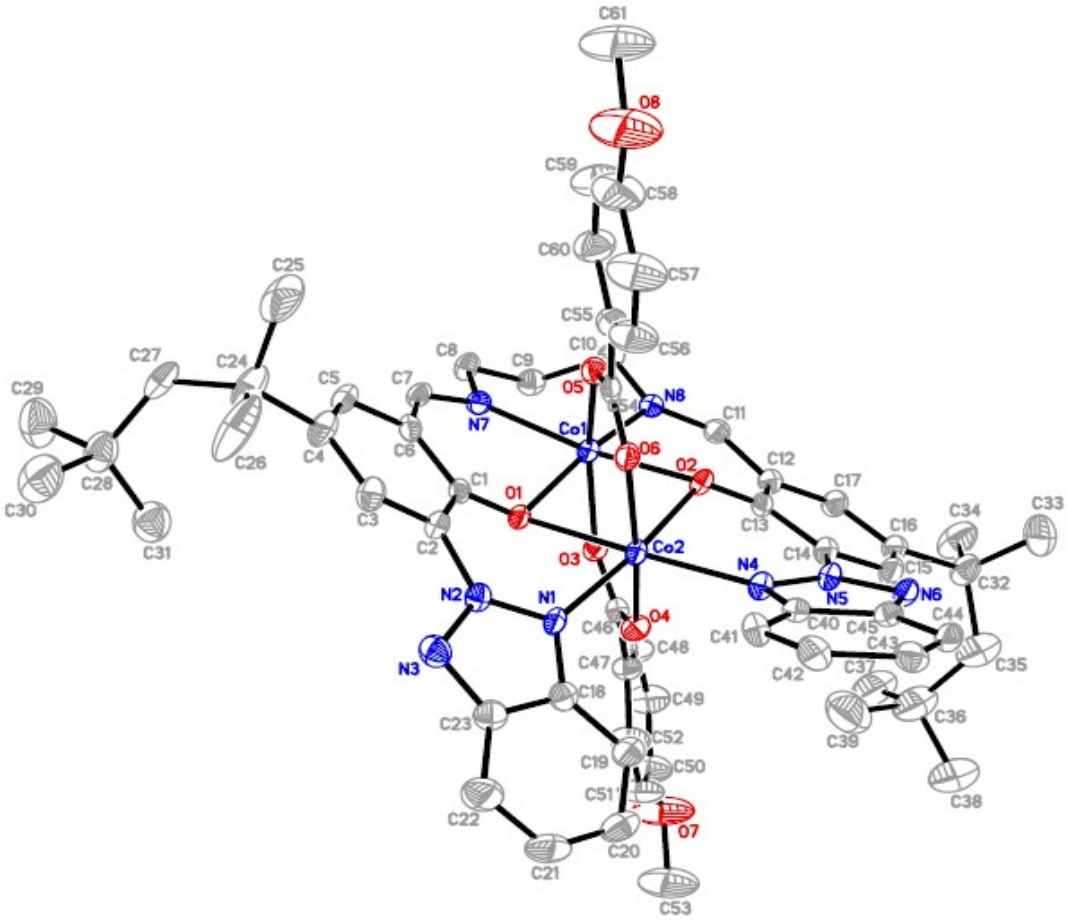

Fig. S6 ORTEP drawing of complex **4** with probability ellipsoids drawn at level 50%. Hydrogen atoms are omitted for clarity. Selected bond lengths (Å) and angles (deg): Co(1)-O(1) 2.056(2), Co(1)-O(2) 2.064(2), Co(1)-N(8) 2.074(3), Co(1)-N(7) 2.093(3), Co(1)-O(5) 2.147(2), Co(1)-O(3) 2.158(2), Co(2)-O(4) 2.059(2), Co(2)-O(6) 2.065(2), Co(2)-O(2) 2.070(2), Co(2)-N(1) 2.084(3), Co(2)-O(1) 2.112(2), Co(2)-N(4) 2.126(3), O(1)-Co(1)-O(2) 95.57(8), O(1)-Co(1)-N(8)167.38(9), O(2)-Co(1)-N(8) 86.06(9), O(1)-Co(1)-N(7) 85.67(9), O(2)-Co(1)-N(7) 169.20(9), N(8)-Co(1)-N(7) 95.08(10), O(1)-Co(1)-O(5) 86.02(8), O(2)-Co(1)-O(5) 81.97(8), N(8)-Co(1)-O(5) 106.59(10), N(7)-Co(1)-O(5) 87.42(9), O(1)-Co(1)-O(3) 82.29(8), O(2)-Co(1)-O(3) 85.02(8), N(8)-Co(1)-O(3) 85.39(9), N(7)-Co(1)-O(3) 105.77(9), O(5)-Co(1)-O(3) 161.57(8), O(4)-Co(2)-O(6) 168.20(9), O(4)-Co(2)-O(2) 87.08(8), O(6)-Co(2)-O(2) 85.60(9), O(4)-Co(2)-N(1) 92.80(9), O(6)-Co(2)-N(1) 93.45(9), O(2)-Co(2)-N(1) 173.63(9), O(4)-Co(2)-O(1) 86.20(8), O(6)-Co(2)-O(1) 85.05(8), O(2)-Co(2)-O(1) 93.71(8), N(1)-Co(2)-O(1) 79.93(9), O(4)-Co(2)-N(4) 92.90(9), O(6)-Co(2)-N(4) 95.40(9), O(2)-Co(2)-N(4) 83.09(9), N(1)-Co(2)-N(4) 103.28(10), O(1)-Co(2)-N(4) 176.72(9).

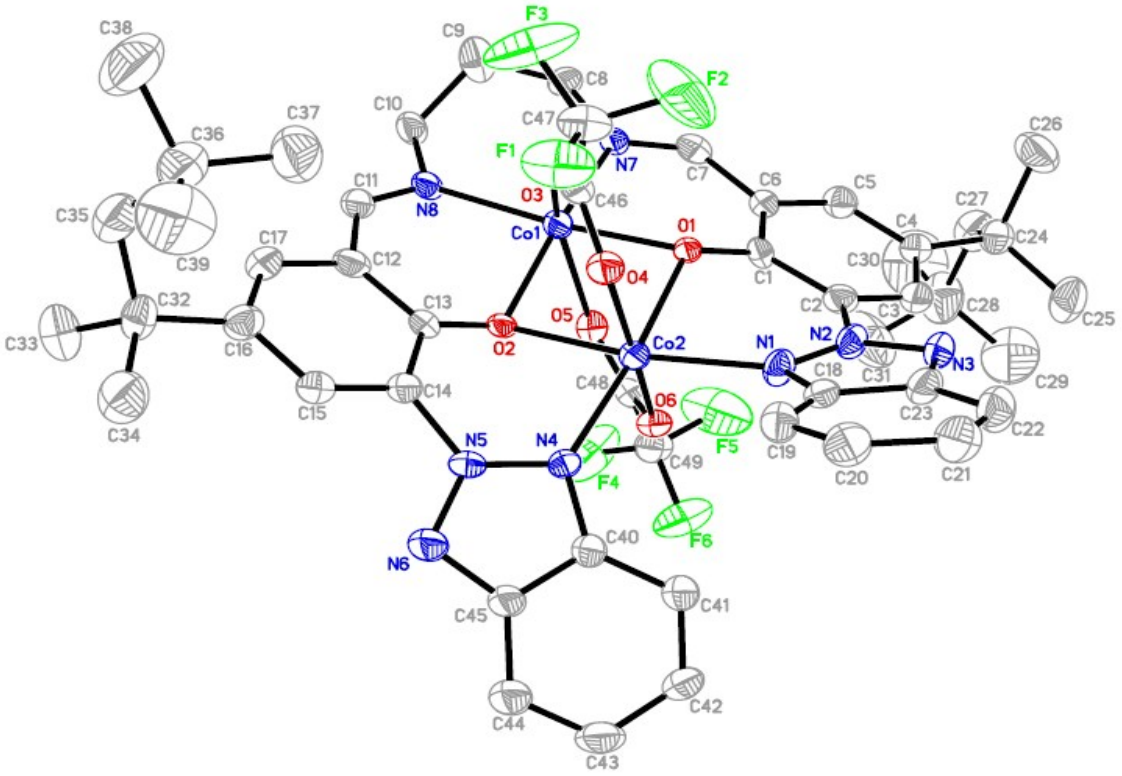

Fig. S7 ORTEP drawing of complex **5** with probability ellipsoids drawn at level 50%. Hydrogen atoms are omitted for clarity. Selected bond lengths (Å) and angles (deg): Co(1)-O(1) 2.042(4), Co(1)-O(2) 2.045(3), Co(1)-N(7) 2.066(4), Co(1)-N(8) 2.074(5), Co(1)-O(3) 2.263(4), Co(1)-O(5) 2.266(4), Co(2)-O(2) 2.073(4), Co(2)-O(4) 2.078(4), Co(2)-O(1) 2.084(3), Co(2)-O(6) 2.085(4), Co(2)-N(4) 2.100(4), Co(2)-N(1) 2.107(5), O(1)-Co(1)-O(2) 92.02(14), O(1)-Co(1)-N(7) 88.38(16), O(2)-Co(1)-N(7) 170.17(17), O(1)-Co(1)-N(8) 169.78(17), O(2)-Co(1)-N(8) 87.92(16), N(7)-Co(1)-N(8) 93.42(18), O(1)-Co(1)-O(3) 80.48(15), O(2)-Co(1)-O(3) 83.96(14), N(7)-Co(1)-O(3) 105.79(17), N(8)-Co(1)-O(3) 89.35(17), O(1)-Co(1)-O(5) 82.30(14), O(2)-Co(1)-O(5) 80.90(15), N(7)-Co(1)-O(5) 89.42(17), N(8)-Co(1)-O(5) 107.76(17), O(3)-Co(1)-O(5) 156.58(14), O(2)-Co(2)-O(4) 86.46(15), O(2)-Co(2)-O(1) 90.03(14), O(4)-Co(2)-O(1) 87.51(15), O(2)-Co(2)-O(6) 88.11(15), O(4)-Co(2)-O(6) 171.94(15), O(1)-Co(2)-O(6) 86.55(15), O(2)-Co(2)-N(4) 84.03(15), O(4)-Co(2)-N(4) 92.70(17), O(1)-Co(2)-N(4) 174.03(16), O(6)-Co(2)-N(4) 92.65(17), O(2)-Co(2)-N(1) 171.28(16), O(4)-Co(2)-N(1) 91.27(18), O(1)-Co(2)-N(1) 81.46(16), O(6)-Co(2)-N(1) 93.22(18), N(4)-Co(2)-N(1) 104.50(18).

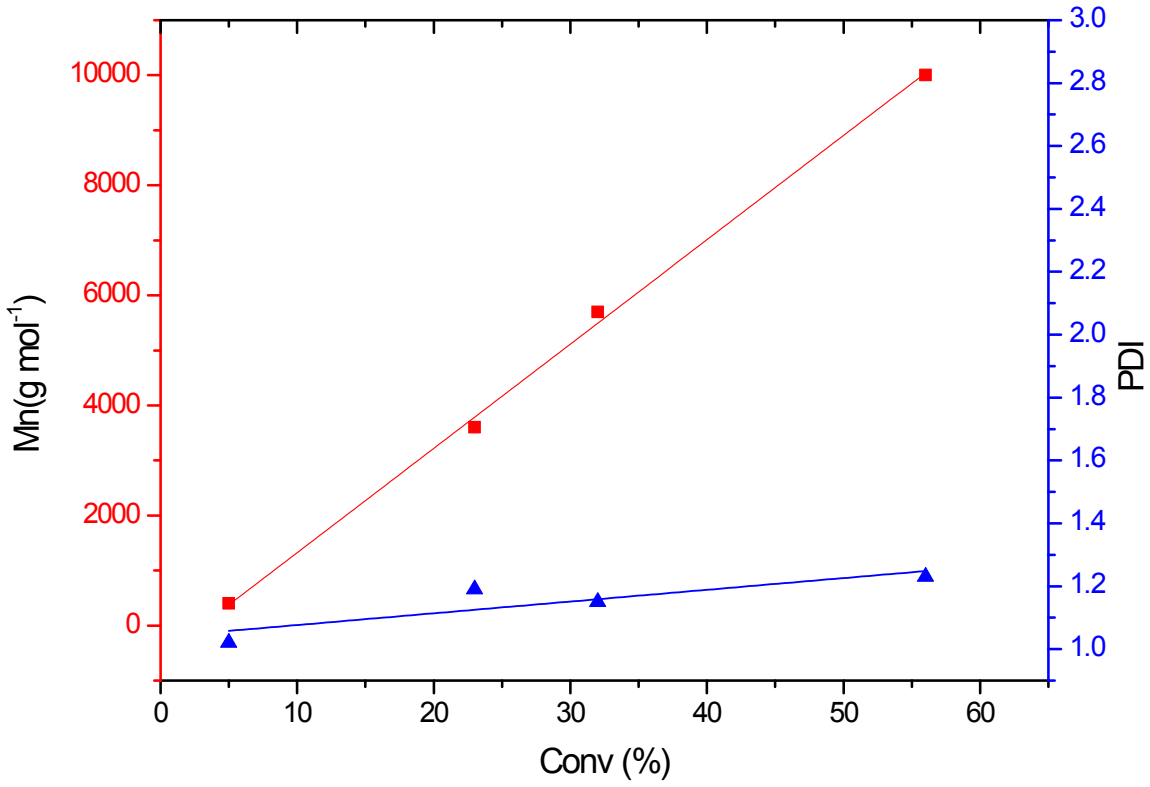

Fig. S8 Plot of M_n (■) and PDI (▲) (determined from GPC analysis) *versus* CHO conversion for the copolymerization of CO_2 and CHO using di-cobalt complex **1** as the catalyst ($[CHO]_0/[\mathbf{1}]_0 = 1600$) at 110 °C and 3.45 MPa CO_2.

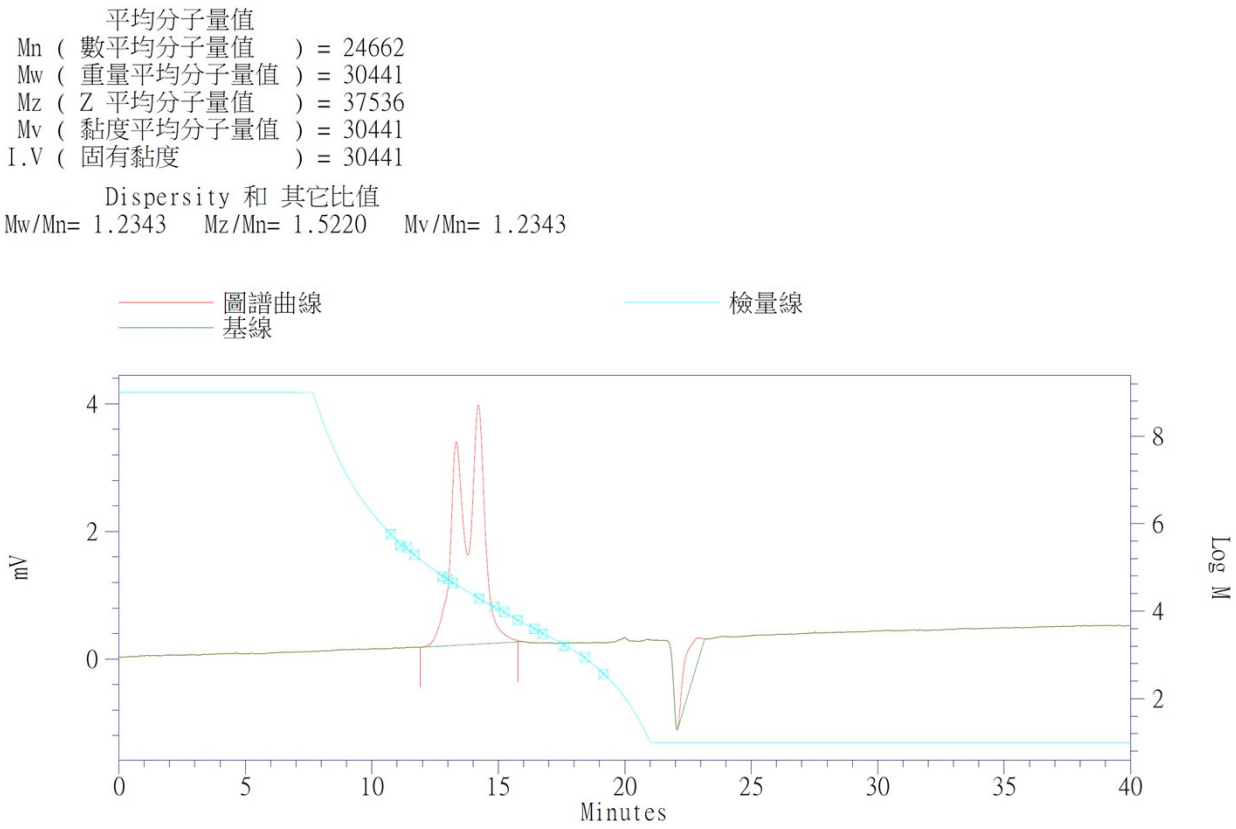

Fig. S9 GPC traces for the produced PCHC with a bimodal molecular weight distribution catalyzed by di-cobalt **1** (Table 2, entry 6).

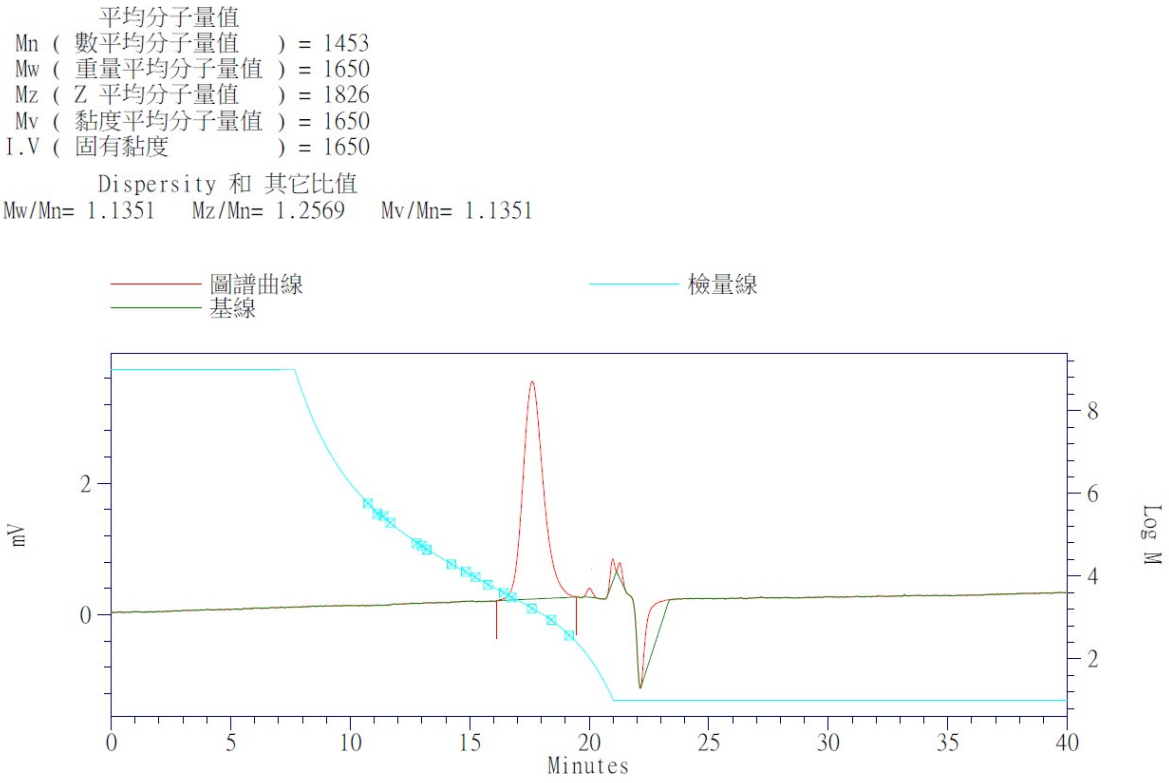

Fig. S10 GPC traces for the produced PCHC polyol with a unimodal molecular weight distribution catalyzed by di-cobalt **1** (Table 2, entry 15).

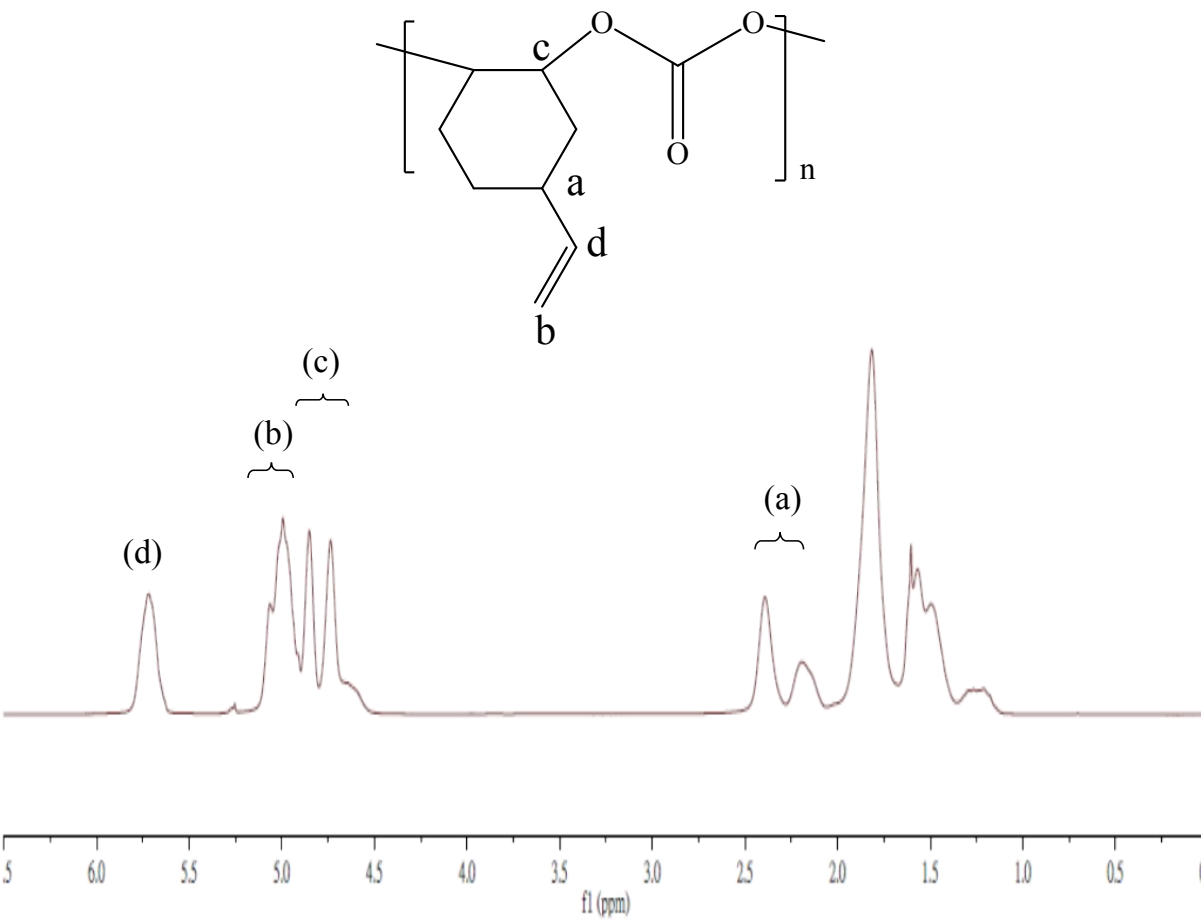

Fig. S11 ^{1}H NMR spectrum of the purified copolymer produced by utilizing di-cobalt complex **1** (Table 2, entry 16) in $CDCl_3$. Peak at δ 4.5−4.9 ppm is assigned to the methine protons in PVCHC, and no significant signal at 3.4−3.8 ppm suggests >99% carbonate repeated units in PVCHC.

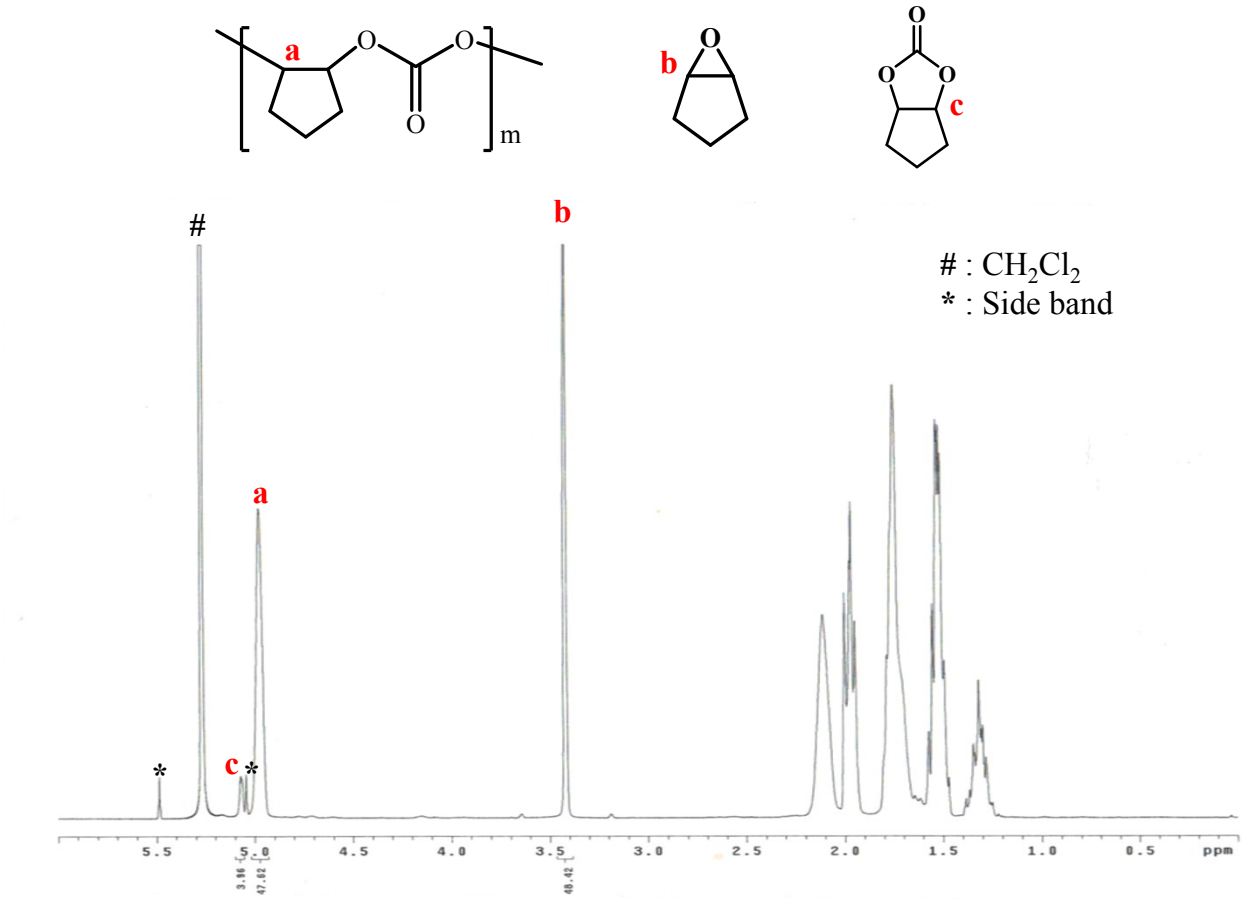

Fig. S12 ^{1}H NMR spectrum of the crude product (Table 2, entry 18) from the reaction mixture of CPO/CO_2 copolymerization by using di-Co complex **1** in $CDCl_3$.

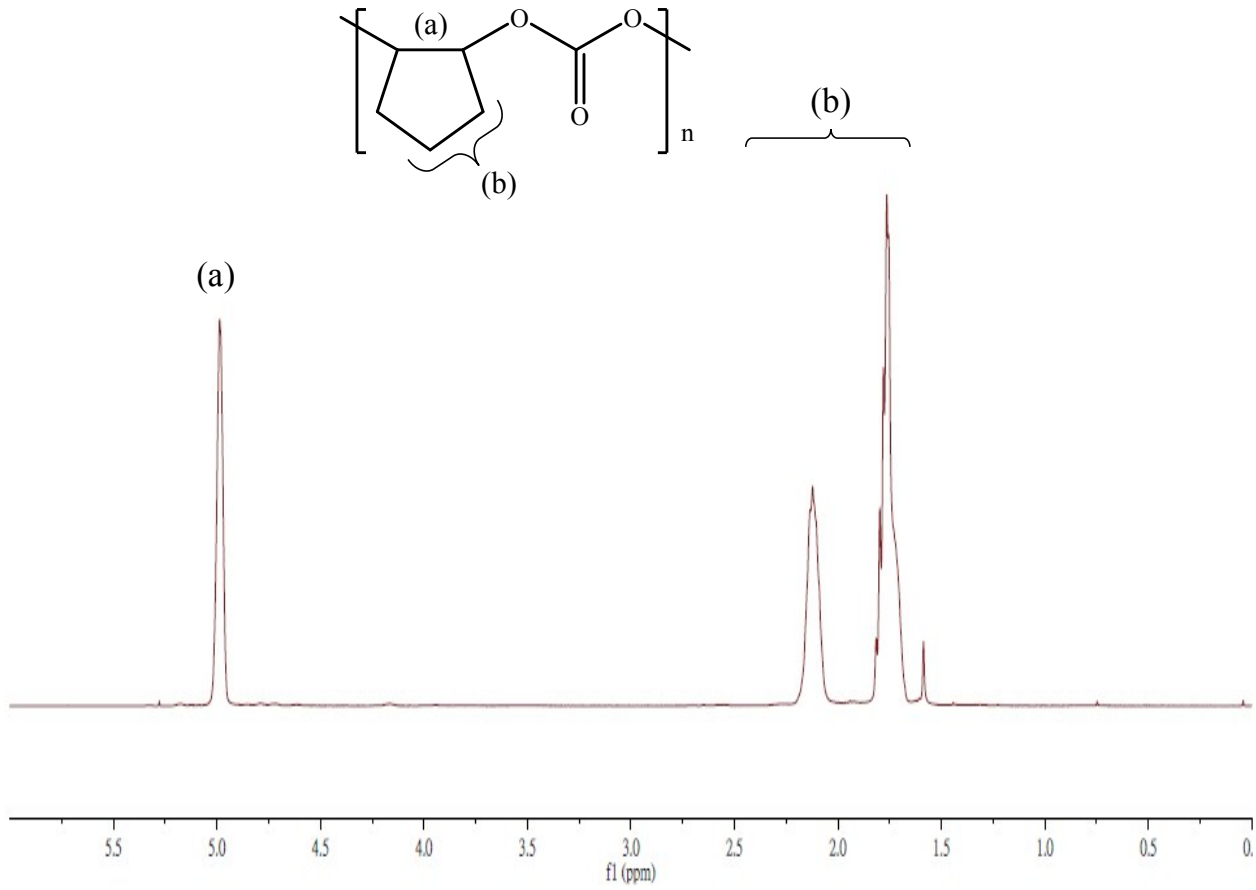

Fig. S13 ^{1}H NMR spectrum of the purified copolymer afforded by utilizing di-cobalt complex **1** (Table 2, entry 17) in $CDCl_3$. Peak at δ = 4.93 ppm is assigned to the methine protons in PCPC, and no obvious signal at 3.6–4.0 ppm confirms >99% carbonate linkages in PCPC.

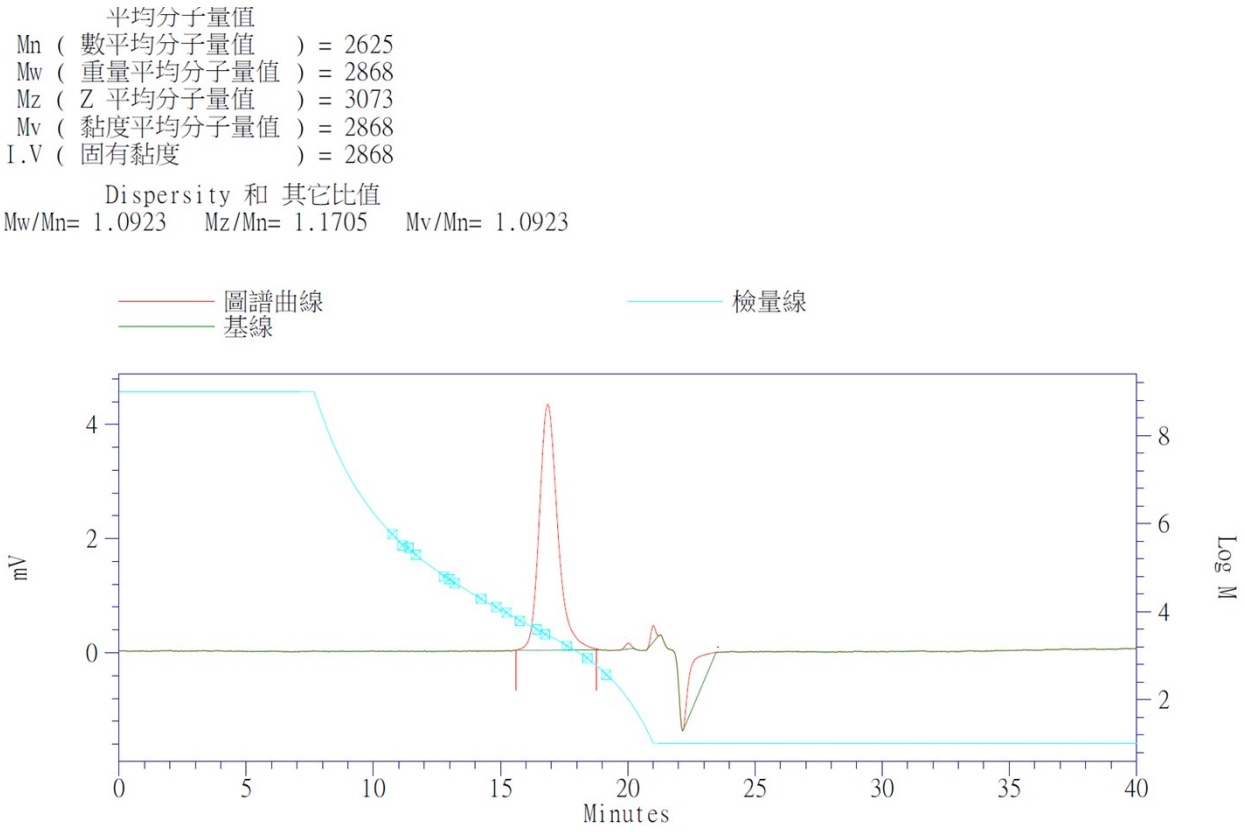

Fig. S14 GPC traces for the produced PCHC polyol with a unimodal molecular weight distribution catalyzed by di-Co **1** in the presence of neopentyl glycol as the CTA (Table 3, entry 2).

(a)

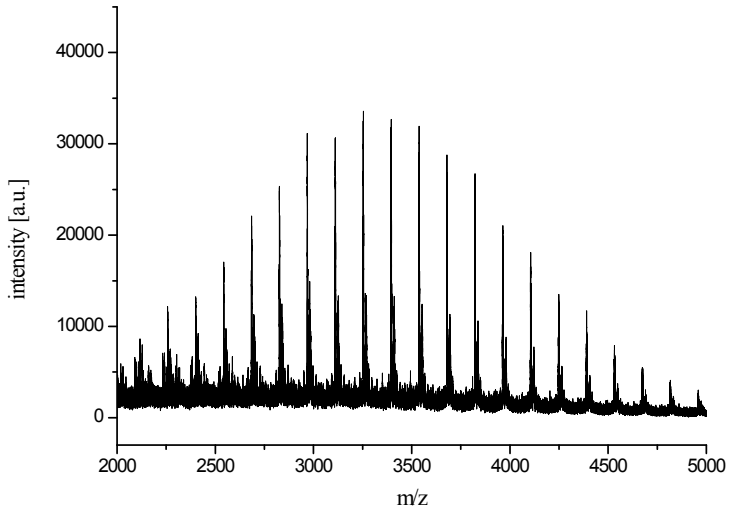

(b)

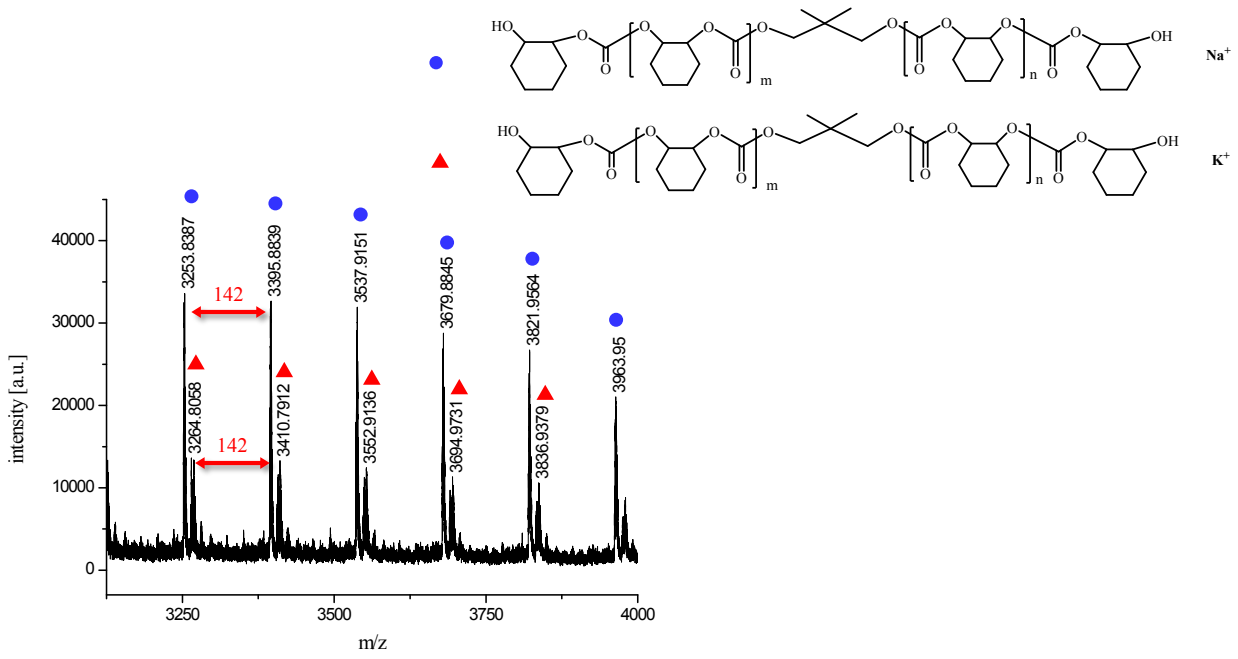

Fig. S15 MALDI-TOF spectrum of the produced PCHC polyol catalyzed by di-Co complex **1** in the presence of neopentyl glycol as the CTA (Table 3, entry 2).

(a)

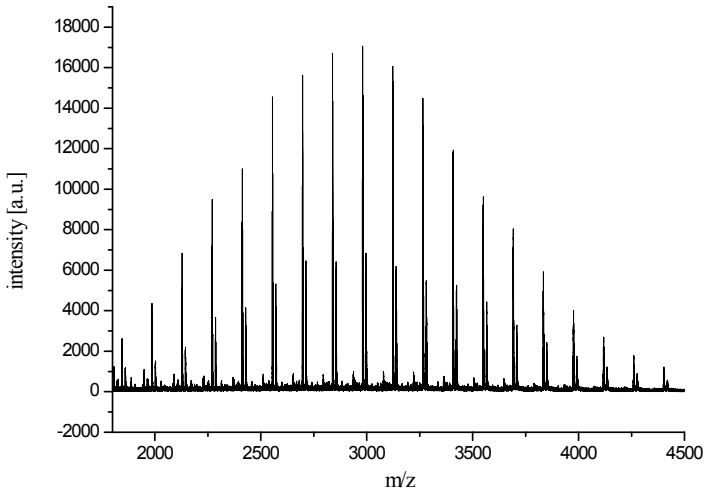

(b)

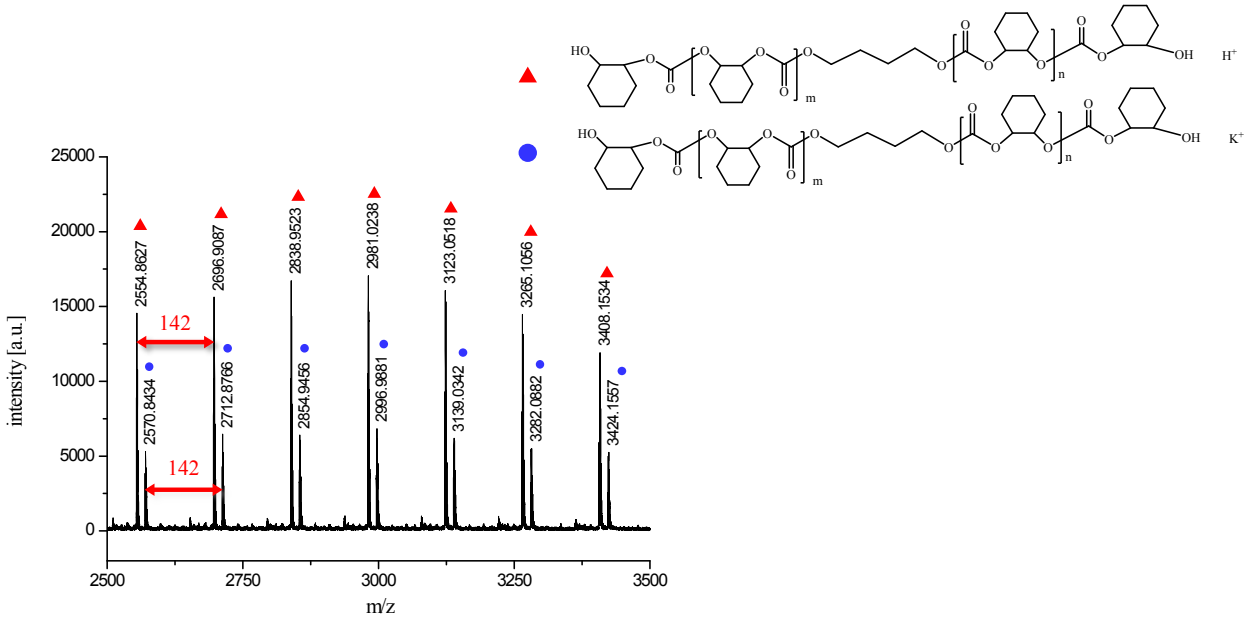

Fig. S16 MALDI-TOF spectrum of the produced PCHC polyol catalyzed by di-Co complex **1** in the presence of BDO as the CTA (Table 3, entry 1).

(a)

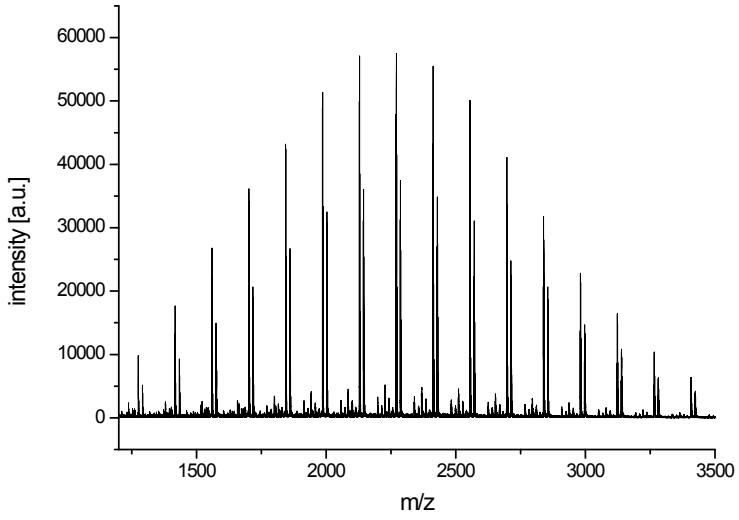

(b)

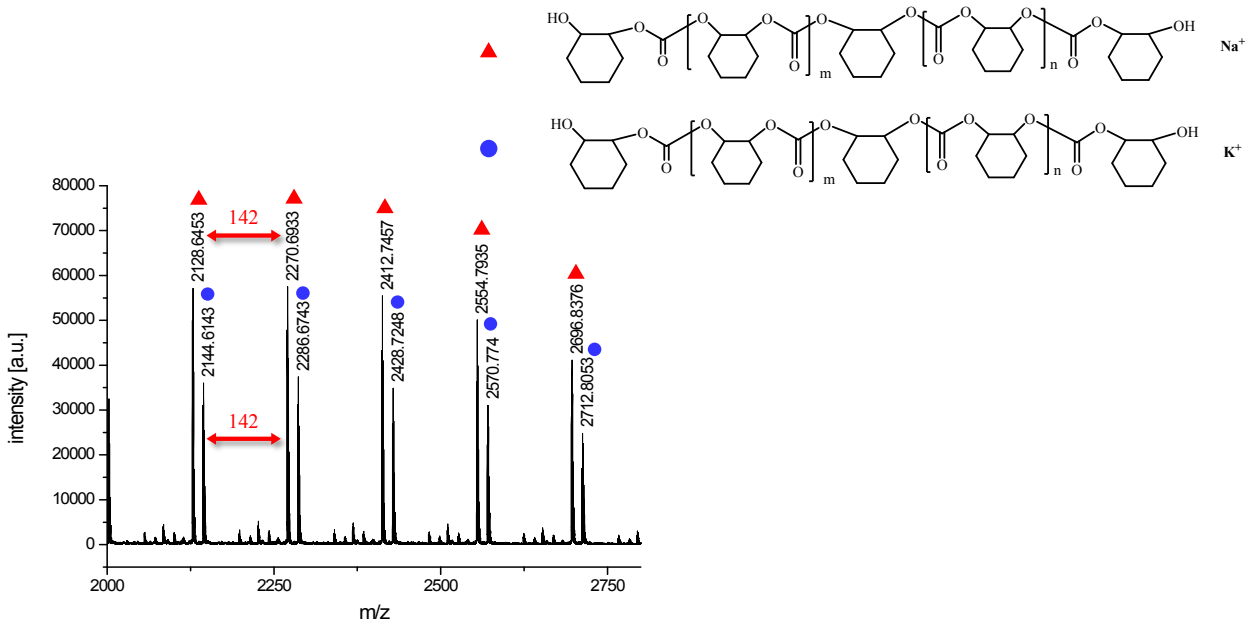

Fig. S17 MALDI-TOF spectrum of the produced PCHC polyol catalyzed by di-Co complex **1** in the presence of BDO as the CHD (Table 3, entry 3).

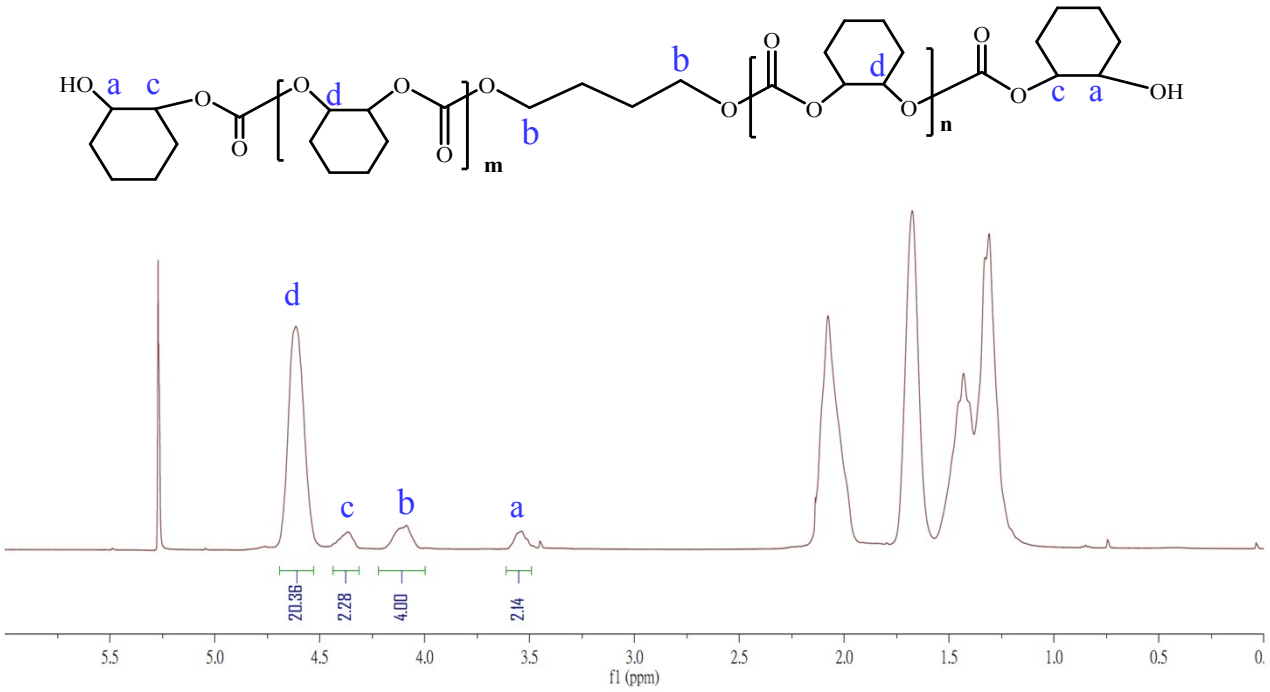

Fig. S18 ^{1}H NMR spectrum ($CDCl_3$) of the purified PCHC polyol catalyzed by di-cobalt complex **1** in the presence of BDO (Table 3, entry 1).

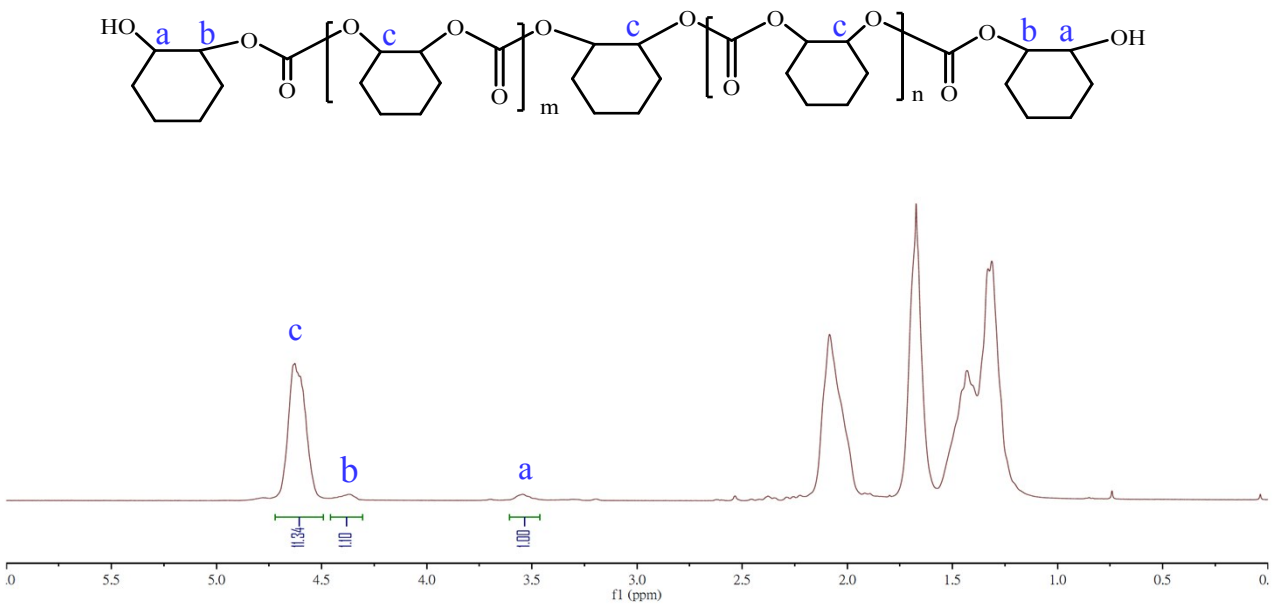

Fig. S19 ^{1}H NMR spectrum ($CDCl_3$) of the purified PCHC polyol catalyzed by di-cobalt complex **1** in the presence of CHD (Table 3, entry 3).

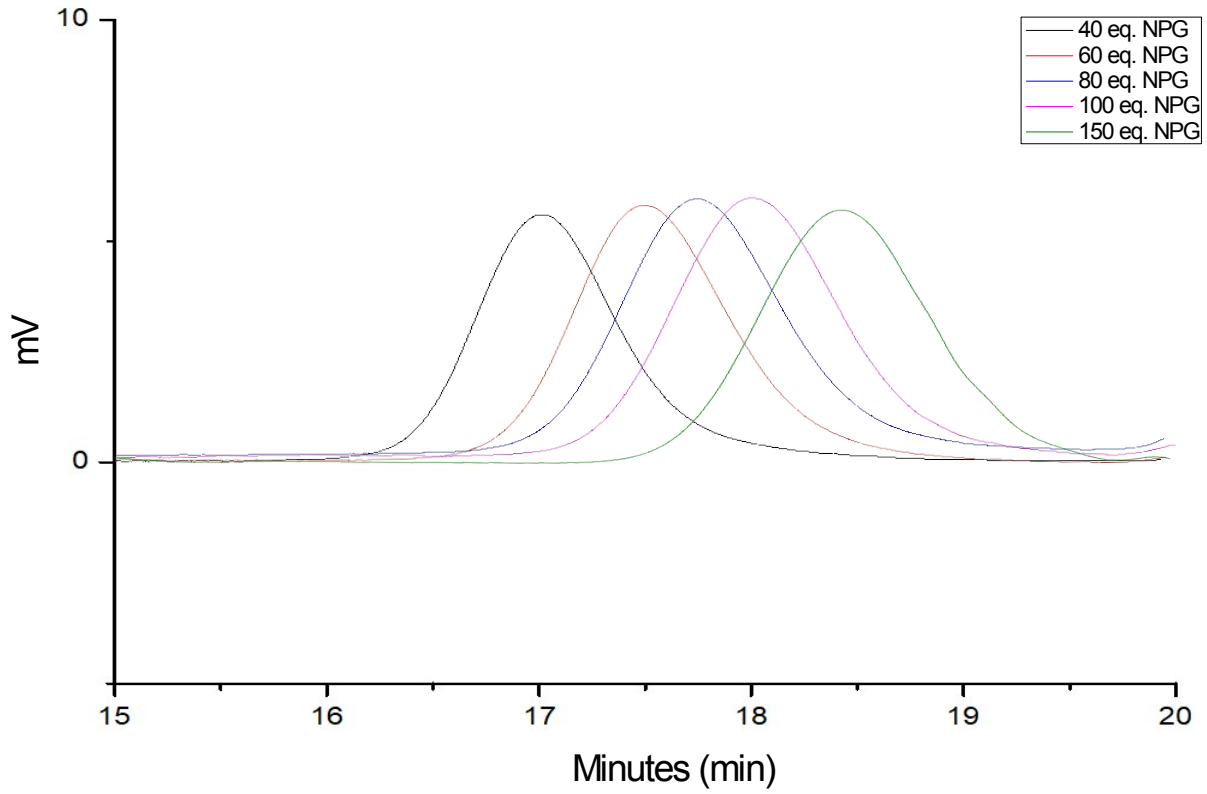

Fig. S20 GPC traces of PCHC polyol samples produced by di-Co complex **1** on increasing the [neopentyl glycol]$_0$/[**1**]$_0$ ratio in a range of 40-150.

Table S1 Key absorbance characteristics for UV–Vis spectra of complexes **1–6** in CH_2Cl_2 ($[M]_0$ = 20 μM) at 25 °C

Complex	Abs, λ_{max}(nm)($\varepsilon/10^4$ M^{-1} cm^{-1})
1	273(5.24), 297(5.49), 395(3.33)
2	271(5.88), 296(5.86), 388(3.67)
3	279(4.78), 300(5.02), 393(2.98)
4	294(6.14), 397(3.54)
5	272(5.56), 295(5.65), 384(3.60)
6	272(8.63), 301(7.22), 389(3.05)

Table S2 Crystallographic data of complexes **1-6**

	1·2CH_2Cl_2	**2**·CH_3OH	**3**·3C_4H_8O
formula	$C_{61}H_{68}Cl_4Co_2N_8O_6$	$C_{60}H_{54}Co_2F_{10}N_8O_7$	$C_{73}H_{86}Co_2F_6N_8O_9$
Formula weight	1268.90	1306.97	1451.36
Temp (K)	150(2) K	150(2) K	150(2) K
Crystal system	Triclinic	Triclinic	Triclinic
Space group	*P*-1	*P*-1	*P*-1
a (Å)	12.5748(7)	13.7628(7)	11.5855(6)
b (Å)	15.9583(10)	14.4760(7)	18.1113(8)
c (Å)	17.0631(12)	17.2399(8)	18.4431(9)
α (deg)	62.939(7)	106.910(2)	75.961(2)
β (deg)	80.725(5)	108.275(2)	80.041(2)
γ (deg)	75.961(5)	104.721(2)	71.644(2)
V(Å^3)	2953.0(4)	2886.2(2)	3543.6(3)
Z	2	2	2
D_{calc}(Mg/m^3)	1.425	1.504	1.360
μ (Mo Kα)(mm^{-1})	0.801	0.668	0.546
F(000)	1316	1340	1520
Reflections collected	26147	138341	72409
No. of parameters	740	861	883
Indep. reflns (R_{int})	10343 (0.0439)	22506 (0.0389)	13902 (0.0504)
$R1[I > 2\sigma(I)]$	0.0510	0.0587	0.0455
w$R2$ $[I > 2\sigma(I)]$	0.1419	0.1600	0.1089
Goodness-of-fit on F^2	0.754	1.028	1.011

Table S2 Crystallographic data of complexes **1-6** (Cont'd)

	4	**5**	**6**
formula	$C_{61}H_{68}Co_2N_8O_8$	$C_{49}H_{54}Co_2F_6N_8O_6$	$C_{59}H_{64}ClCo_2N_8O_{10}$
Formula weight	1159.09	1082.86	1198.49
Temp (K)	150(2) K	150(2) K	150(2) K
Crystal system	Triclinic	Triclinic	Triclinic
Space group	*P*-1	*P*-1	*P*1
a (Å)	12.7268(4)	11.9469(9)	10.7521(4)
b (Å)	15.9231(6)	15.2398(11)	11.9322(6)
c (Å)	16.6055(5)	15.5352(12)	14.3164(7)
α (deg)	107.835(3)	111.573(2)	106.321(2)
β (deg)	102.906(3)	97.145(3)	97.244(2)
γ (deg)	105.922(3)	95.552(3)	106.744(2)
V(Å^3)	2901.65(17)	2578.6(3)	1644.59(13)
Z	2	2	1
D_{calc}(Mg/m^3)	1.327	1.395	1.210
μ (Mo Kα)(mm^{-1})	0.633	0.720	0.602
F(000)	1216	1120	625
Reflections collected	49549	37795	49742
No. of parameters	724	650	707
Indep. reflns (R_{int})	11399 (0.0503)	10471 (0.0556)	15907 (0.0314)
$R1[I > 2\sigma(I)]$	0.0541	0.0859	0.0374
w$R2$ $[I > 2\sigma(I)]$	0.1339	0.2006	0.0989
Goodness-of-fit on F^2	1.027	1.004	0.860